Stability of Weyl points in magnetic half-metallic Heusler compounds

Stanislav Chadov,* Shu-Chun Wu, and Claudia Felser
Max-Planck-Institute for Chemical Physics of Solids, D-01187 Dresden, Germany

Iosif Galanakis†
Department of Materials Science, School of Natural Sciences, University of Patras, GR-26504 Patra, Greece
(Received 11 February 2017; published 24 July 2017)

We employ *ab initio* fully relativistic electronic structure calculations to study the stability of the Weyl points in the momentum space within the class of the half-metallic ferromagnetic full Heusler materials, by focusing on Co_2TiAl as a well-established prototype compound. Here we show that both the number of the Weyl points together with their k-space coordinates can be controlled by the orientation of the magnetization. This alternative degree of freedom, which is absent in other topological materials (e.g., in Weyl semimetals), introduces functionalities that are specific for the class of half-metallic ferromagnets. Of special interest are crossing points which are preserved irrespective of any arbitrary rotation of the magnetization axis.

DOI: 10.1103/PhysRevB.96.024435

I. INTRODUCTION

The transfer of concepts between different disciplines and fields of science has triggered the appearance and growth of new research fields. One of the most striking recent examples is the notion of topology in condensed-matter physics and materials science. Following the discovery of topological insulators (see Refs. [1] and [2] and references therein), it was suggested theoretically that the band structures of Na_3Bi and Cd_3As_2 show Dirac-like energy cones at the Fermi surface [3,4]. Theoretical predictions were confirmed in 2014 and the compounds were named Dirac semimetals [5]. These findings initiated even more intense interest in the topological effects and the role of the breaking of symmetries was investigated [6].

In condensed-matter physics, the spin degeneracy at a general k point is protected by the coexistence of time-reversal symmetry and inversion symmetry, the so-called Kramer degeneracy. Breaking only one of the two symmetries breaks a Dirac point into two Weyl points (WPs) of opposite chirality. Thus there are two types of Weyl semimetals: (a) magnetic Weyl semimetals where inversion symmetry is kept and (b) nonmagnetic noncentrosymmetric ones where time-reversal symmetry is kept (for an extensive review of Weyl semimetals, see Ref. [7]). Two types of WPs can occur: type-I, which are isolated points in the Brillouin zone, and type II, which represent a closed loop. There are also rare cases of semimetals, such as $SrSi_2$, where both the inversion and time reversal symmetries are broken, leading to the formation of an exotic double Weyl fermion [8].

The search for WPs in magnetic systems is a nontrivial task. First, experimentally angle-resolved photoemission spectroscopy (ARPES) measurements of the magnetic Weyl materials are very difficult due to the complex domain structure and thus there is still no material definitely confirmed to be a magnetic Weyl semimetal [7]. Second, theoretically, the search for WPs in the three-dimensional (3D) reciprocal space is rather complicated since the WPs might be general points of the Brillouin zone and not just along high-symmetry axes. Similar manifolds might be formed also by normal degeneracies along the high-symmetric directions. In the case of the magnetic systems, such symmetry analysis requires the Shubnikov type-II groups and becomes even more complicated.

Among the Heusler compounds [9,10], the ones being half-metallic ferromagnets have attracted considerable attention due to their potential applications in spintronics [11,12]. Their most striking characteristic is the so-called Slater-Pauling behavior of the total spin magnetic spin moment, which scales linearly with the number of valence electrons [13,14]. This large family provides flexible possibilities to tune their electronic structure, e.g., by shifting the Fermi energy with chemical composition. Due to the very large number of Heusler compounds, it is natural to search for WPs either in the nonmagnetic semi-Heuslers which crystalize in a noncentrosymmetric lattice [15] or among the regular magnetic ones crystallizing in the $L2_1$ structure [space group $Fm\bar{3}m$ (225)]. Their cubic crystalline structure results in a low magnetocrystalline anisotropy at zero temperature for which electronic structure calculations are carried out. Thus, at low temperature, their magnetization can be easily manipulated using an external magnetic field, both in single-crystalline as well as polycrystalline samples, while at more elevated temperatures, the thermal energy would overcome the magnetocrystalline energy and the samples would show practically no easy axis. Since the $L2_1$ structure is centrosymmetric, the appearance of magnetism breaks the time-reversal symmetry, possibly leading to the appearance of WPs.

II. MOTIVATION AND COMPUTATIONAL DETAILS

In 2016, three articles appeared that focused on the WPs in magnetic Heusler compounds. Kübler and Felser suggested that in the case of Co_2MnAl, the appearance of a large anomalous Hall effect is linked to four WPs just above the Fermi level [16]. Wang and collaborators studied several Co-based Heusler compounds focusing especially on Co_2ZrSn and found that when the magnetization is along the [110] direction, there are at least two WPs close to the Fermi level separated by a large distance in the reciprocal space giving rise to

*stanislav.chadov@cpfs.mpg.de
†galanakis@upatras.gr

well-defined Fermi arcs [17]. Finally, Chang and collaborators studied the Co_2Ti(Si, Ge, or Sn) compounds and found another two WPs in the $K - \Gamma$ direction which are different than the ones mentioned just above [18]. *Ab initio* calculations in both Refs. [17] and [18] revealed that the different magnetization axes cannot be energetically distinguished probably due to the very high symmetry of the lattice. Thus the important question arises concerning the stability of the observed WPs with respect to the magnetization axis which can be rotated due to external magnetic fields. The answer to this question is primordial for applications since in most cases polycrystalline films are used and thus an external magnetic field would oblige the different domains to have their magnetization along a different crystallographic axis and thus the number of interesting band crossings might be substantially reduced. The most interesting band crossings would be those which survive upon arbitrary rotation of the magnetization.

To study them, we consider a typical representative of the Co_2-based Heusler family, namely Co_2TiAl, which has been well established experimentally and theoretically as a good half-metallic ferromagnet obeying the Slater-Pauling rule; it has 25 valence electrons per formula unit with a total spin magnetic moment of 1 μ_B per formula unit [13]. We have also studied Co_2TiSi and Co_2VAl which have 26 valence electrons, and results and conclusions were also similar for them with the only noticeable difference being that the WPs were lower in energy due to the extra electron as expected; the Fermi level in Heuslers can be varied within a rather wide range by changing the chemical composition [12]. In all cases, we have used the experimental lattice constants [19,20]. To perform the electronic structure calculations, we employed the full-potential nonorthogonal local-orbital minimum-basis band structure scheme (FPLO) [21] within the generalized gradient approximation (GGA) [22]. We performed first scalar-relativistic and then fully relativistic calculations where the Dirac-like analog to Kohn-Sham equations is solved [21]. As the quantization axis, we have considered three cases: [001], [110], and [111]. During the self-consistency, for the Brillouin zone integration, a Monkhorst-Pack $30\times30\times30$ grid has been used [23]. Total energies have been converged with an accuracy of 10^{-8} in Hartree. Band structure plots have been plotted within the $k_z = 0$ plane for all cases considering a very dense division of 500 **k** points between two consecutive high-symmetry points.

III. RESULTS AND DISCUSSION

We will start our discussion from the scalar-relativistic band structure obtained for Co_2TiAl and presented in Fig. 1. In this case, we can decompose the bands in pure majority- and minority-spin character. The minority-spin band structure presents a direct gap at the Γ point of about 0.5 eV, typical for half-metallic Heusler compounds, and the total spin magnetic moment of 1 μ_B is in agreement with the Slater-Pauling rule [13]. All high-symmetry points in Fig. 1 have been chosen within the $k_z = 0$ plane perpendicular to the z axis; Γ, X, W, and K coordinates in the reciprocal space are [0 0 0], [1 0 0], [1 $\frac{1}{2}$ 0], and [$\frac{3}{4}$ $\frac{3}{4}$ 0], respectively, in $\frac{2\pi}{a}$ units where a is the lattice constant. Due to the existence of three transition-metal atoms per formula unit, there is a very large umber of d bands

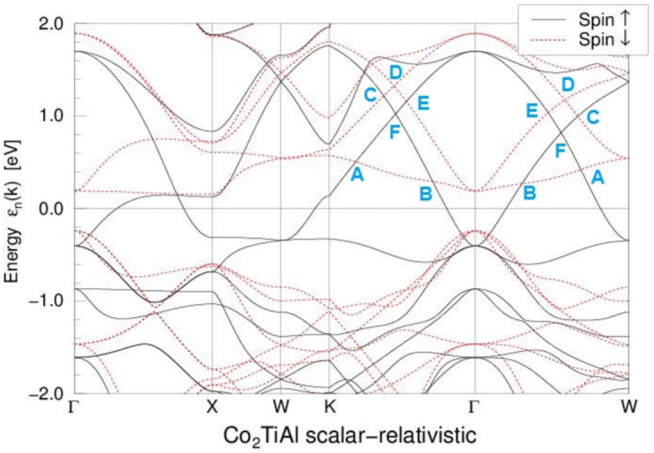

FIG. 1. Calculated electronic band structure of Co_2TiAl using the scalar-relativistic formalism. The zero energy in the vertical axis is the Fermi level. We have denoted the six crossing points of interest with the symbols A–F. Note that all high-symmetry points are within the $k_z = 0$ plane.

around the Fermi level in a narrow energy region (for the character of the bands, see Ref. [13]). As a result, several crossings which can be considered as potential WPs occur not only along the high-symmetry lines shown in Fig. 1, but in the whole Brillouin zone.

In order to make our study possible, we have focused on six crossing points along the $K - \Gamma$ direction which have their exact symmetry analog in the $\Gamma - W$ direction, as shown in Fig. 1. The Γ-K direction has been proposed to contain the WPs according to Refs. [17] and [18]. The energy window under study which contains the relevant WPs is between the Fermi level and 2 eV above it ($0 < E - E_F < 2$ eV), as shown in Fig. 1. A detailed analysis of the band structure using the so-called fat band scheme [24] revealed the character of the bands which cross, and we present in Fig. 2 the bands' orbital character as deduced using the fat band scheme. The minority-spin band at the A and B points, which have been proposed to be WPs in Ref. [18], belongs to the double-degenerate e_u

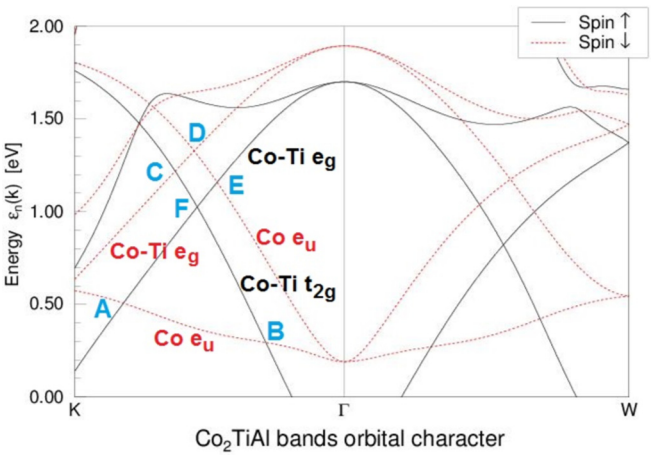

FIG. 2. Orbital character of the bands which cross at the six points along the $K - \Gamma - W$ direction shown in Fig. 1.

bands, which have their weight exclusively at the Co atoms (see Ref. [13] for an extended discussion of the character of the bands). This band at point B crosses a majority-spin band made up of states belonging to the triple-degenerate antibonding t_{2g} states with most of their weight at the Ti atom, and at point A crosses a majority-spin band belonging to the double-degenerate antibonding e_g states, again with most of their weight at the Ti atoms. After the B point, the majority-spin t_{2g} band crosses the antibonding majority-spin e_g band at point F and the minority-spin e_g band at point C. The other minority-spin e_u state discussed in the beginning also crosses these two states at points E and D. Thus all six points arise due to crossing of bands of different spin or orbital character.

As a first step using the fully relativistic formalism, we have computed the band structure choosing as quantization axis the [100] and [001], simulating in this way the effect of the external magnetic field on the direction of the magnetization. We present our results in Fig. 3, focusing above the Fermi level and in the $K - \Gamma - W$ direction. To facilitate the discussion, we

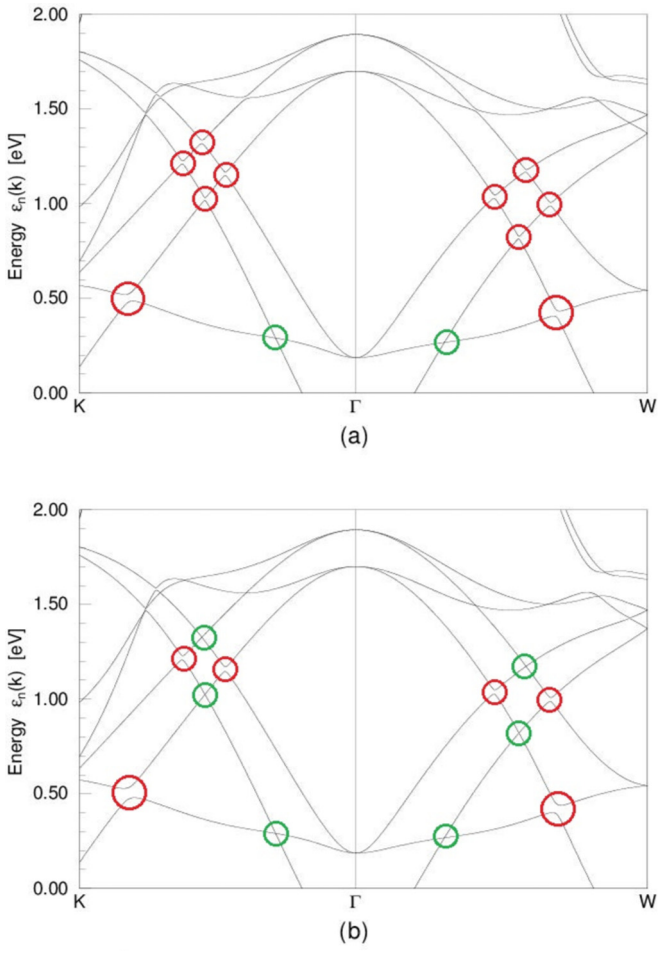

FIG. 3. (a) Calculated electronic band structure of Co_2TiAl using the fully relativistic formalism and setting the quantization axis to be the [100]. (b) Same as (a), with [001] as the quantization axis. In both cases, the zero energy in the vertical axis is the Fermi level. We have encircled with red colors the crossing points where the degeneracy is lifted and crossing no longer occurs, and with green color the ones where the crossing is preserved.

have encircled with red color the cases where the degeneracy is lost and there is no longer any crossing and with green color the cases where the crossing is preserved. In the Dirac relativistic formalism, spin is no longer a good quantum number and thus we cannot project our band structures on spin. When the quantization axis is along the [100] direction, only the M_x mirror plane which is normal to the [100] direction and the fourfold C_{4x} rotational axis survive. As a result, in the $k_z = 0$ plane, only the WP at points B is preserved. The $k_y = 0$ is equivalent to the $k_z = 0$ plane and the question is what happens in the $k_x = 0$ plane normal to the [100] axis. To answer this question, we have considered as quantization axis the [001] and now the $k_z = 0$ plane in the lower panel of Fig. 3 corresponds to the $k_x = 0$ plane in the case of the [100] axis. We can see that now at the points D and F, the degeneracy is preserved. Thus, in magnetic materials, the situation is much more complicated than the one expected for magnetic semimetals [7]. We have performed fully relativistic calculations also considering the [110], [011], and [111] as the quantization axis. Now the symmetry operations are different in each case, e.g., in the [110] case, the symmetry operations—except the inversion symmetry—which are preserved are the mirror plane M_{xy} which is normal to the [110] axis and the $C_2^{[110]}$ rotation. Calculated band structures suggest that different crossing points are conserved in each case.

To further analyze the behavior of the crossing points, we focused on the ones marked as A–D in Fig. 1 since F is equivalent to D and E to C. In this case, there are 12 equivalent Γ-K directions allowed by the $Fm\bar{3}m$ space group. In order to distinguish between spin states in the fully relativistic regime, we have employed the Korringa-Kohn-Rostoker (KKR) electronic structure method employing relativistic spin-projection operators [25]. For the usual spin-polarized case without the spin-orbit coupling, KKR yields a similar band structure to the FPLO one, presented in Fig. 1. In order to track the appropriate changes induced by the spin-orbit coupling with respect to the simply spin-polarized ones, we will simultaneously depict all 12 points of each type (A–D) on the same Γ-centered sphere in the 3D k space, by tuning its radius precisely to host the given point type (and simultaneously tuning the corresponding energy). Such representation allows one to compare their character together with its evaluation by changing the magnetization orientation (see Fig. 4).

In Fig. 4, we consider three distinct orientations of the magnetization: $\vec{M} \parallel [001]$, [111], and [110]. We also decompose the spectral density into the majority and minority spin (using red and blue colors for the spectral density, respectively). By considering, for example, the sphere containing the point A (A sphere), we see that it has an anticrossing character for all k directions and magnetization orientations except for $\vec{M} \parallel [110]$, where it keeps crossing along $\vec{k} \parallel [110]$ (and along the equivalent $[\bar{1}\bar{1}0]$ which is just hidden behind). One partially observes this also in the corresponding $E(k)$ plots (shown only for two nonequivalent directions): encircling of the A points is shown in red everywhere (anticrossing) except of $\vec{k} \parallel [110]$ for the $\vec{M} \parallel [110]$ case (green). This means that by taking the polycrystalline case, the overall contribution of the A crossing into the transport properties (provided it is tuned to the Fermi energy) will be drastically reduced. The same situation occurs for the C type, which keeps crossing

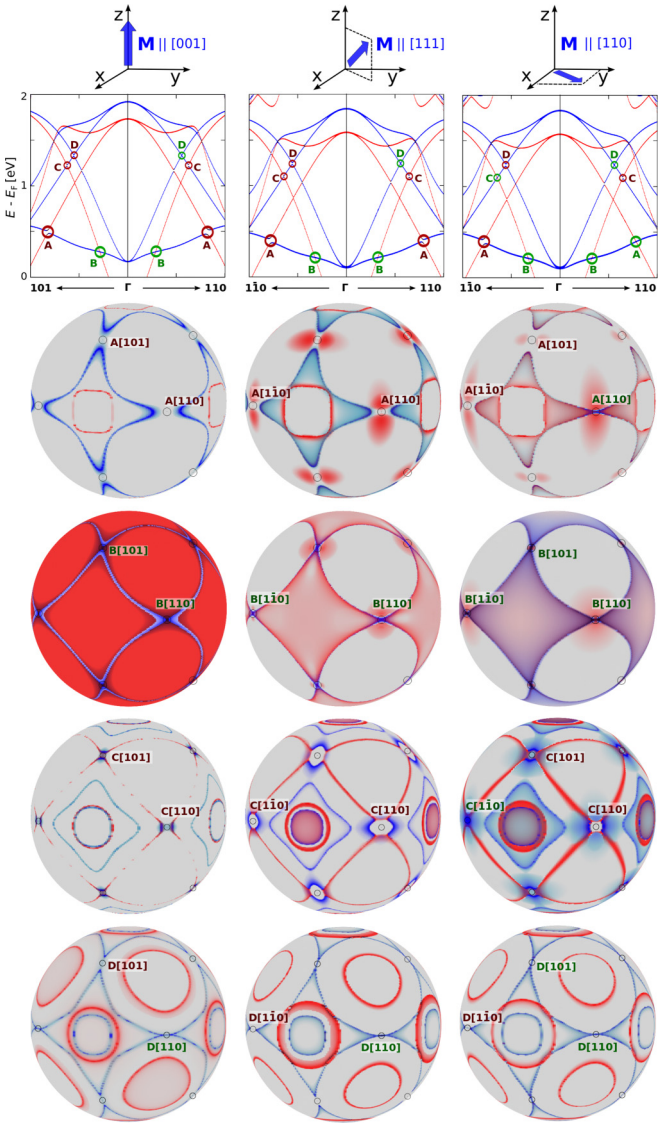

FIG. 4. Upper panel: Fully relativistic band structures of Co_2TiAl computed along the K-Γ-K' k path (Γ-K and Γ-K' directions are denoted explicitly) for three orientations of the magnetization **M**, i.e., [001], [111], and [110]. (E,k) points of interest (of A–D type) are emphasized by green or red circles depending on their crossing or anticrossing character, respectively. Minority- and majority-spin states are colored as red and blue, respectively. Lower panels: The corresponding nonequivalent points of each type, plotting the spectral weight on Γ-centered spheres in 3D k space (green letters mark crossing character and black letters mark anticrossing character). Red and blue lines and surfaces mark minority- and majority-spin states as in the upper panel; note that at some parts of the spheres, there is superposition of the two different spin states and thus of the two colors used to denote them.

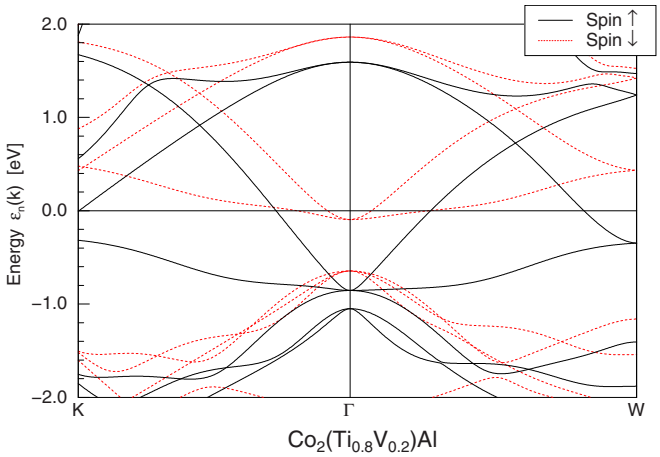

FIG. 5. Calculated electronic band structure of $Co_2(Ti_{0.8}V_{0.2})Al$ using the scalar-relativistic formalism within the virtual crystal approximation for a strained lattice (see text for details). Note that now the B points are located exactly at the Fermi level which is the zero energy in the vertical axis.

only along $\vec{k} \parallel [1\bar{1}0]$ (and $[\bar{1}10]$) for the $\vec{M} \parallel [110]$ case. The intermediate situation occurs for the D type, which has a pure minority-spin character: for $\vec{M} \parallel [001]$. It gives crossing characters in four xy directions, i.e., [110], $[\bar{1}\bar{1}0]$, $[1\bar{1}0]$, and $[\bar{1}10]$, six crossings in the case of $\vec{M} \parallel [111]$, and six crossings in the case of $\vec{M} \parallel [110]$. In contrast to A, C, and D, the B point exhibits the most universal behavior: it preserves the crossing character in all k directions for all magnetization orientations.

The results presented above indicate that by tuning the Fermi energy to the B point, an efficient overall transport response might be achieved even in the polycrystalline case. The tuning of the B point at the Fermi level can be achieved by simultaneously doping Co_2TiAl with V instead of Ti and introducing strain in the lattice [26]. If only doping is carried out, the extra electronic charge occupies majority-spin states pushing the bands lower in energy. But this does not guarantee that the Fermi level is shifted enough so that the B points are close to it. In order to achieve it, one should also apply stress which will shift the Fermi level higher in energy with respect to the minority-spin bands. To demonstrate this, we have plotted in Fig. 5 the scalar-relativistic band structure for the $Co_2(Ti_{0.8}V_{0.2})Al$ compound using the virtual crystal approximation to account for the doping at the Ti sites. Simultaneously, we have applied a small stress by decreasing the in-plane lattice constants by 0.15 Å with respect to the one used for the calculations above and simultaneously increasing the out-of-plane lattice constant to keep the unit-cell volume constant; experimentally this can be achieved by growing on a suitable substrate. As can be seen in Fig. 5, the B points in the case of the disordered compounds are now located exactly at the Fermi level and thus efficient electronic transport can be achieved.

IV. SUMMARY AND CONCLUSIONS

Employing *ab initio* calculations within the fully relativistic Dirac formalism, we studied the stability of Weyl points in magnetic half-metallic Heusler compounds using Co_2TiAl as a prototype. Our results suggest that the preservation of the crossing points observed in the scalar-relativistic band structure strongly depends on the orientation of the quantization axis due to the broken symmetry operations. Moreover, due to symmetry reasons, the band structure within the $k_x = 0$,

$k_y = 0$, and $k_z = 0$ plane differs for a given quantization axis, making the identification of the Weyl points which are preserved even more complex. In the case of Co_2TiAl, we found that there is a crossing which is invariant to the rotation of the magnetization axis and thus it is a real Weyl point.

Our results clearly show that external magnetic fields, which pin the quantization axis in magnetic half metals, affect the number and the momentum-space location of Weyl points, offering different possibilities not present in conventional Weyl semimetals in the field of topological materials.

ACKNOWLEDGMENTS

The authors acknowledge fruitful discussion with G. H. Fecher and J. Kübler. I.G. thanks C.F. for her hospitality during his stay at MPI-CPfS, Dresden, where part of the work was done.

[1] Y. Ando, Topological insulator materials, J. Phys. Soc. Jpn. **82**, 102001 (2013).
[2] A. Bansil, H. Lin, and T. Das, *Colloquium*: Topological band theory, Rev. Mod. Phys. **88**, 021004 (2016).
[3] Z. J. Wang, Y. Sun, X. Q. Chen, C. Franchini, G. Xu, H. M. Weng, X. Dai, and Z. Fang, Dirac semimetal and topological phase transitions in A_3Bi (A = Na, K, Rb), Phys. Rev. B **85**, 195320 (2012).
[4] Z. J. Wang, H. M. Weng, Q. S. Wu, X. Dai, and Z. Fang, Three dimensional Dirac semimetal and quantum transport in Cd_3As_2, Phys. Rev. B **88**, 125427 (2013).
[5] Z. Liu *et al.*, Discovery of a three-dimensional topological Dirac semimetal, Na3Bi, Science **343**, 864 (2014).
[6] B. Bradlyn, J. Cano, Z. Wang, M. G. Vergniory, C. Felser, R. J. Cava, and B. A. Bernevig, Beyond Dirac and Weyl fermions: Unconventional quasiparticles in conventional crystals, Science **353**, aaf5037 (2016).
[7] H. Weng, Xi Dai, and Z. Fang, Topological semimetals predicted from first-principles calculations, J. Phys.: Condens. Matter **28**, 303001 (2016).
[8] S.-M. Huang *et al.*, New type of Weyl semimetal with quadratic double Weyl fermions, Proc. Natl. Acad. Sci. USA **113**, 1180 (2016).
[9] F. Heusler, Kristallstruktur und Ferromagnetismus der Mangan-Aluminium-Kupferlegierungen, Verh. Dtsch. Phys. Ges. **12**, 219 (1903).
[10] F. Heusler and E. Take, The nature of the Heusler alloys, Phys. Z. **13**, 897 (1912).
[11] A. Hirohata and K. Takanashi, Perspectives of Heusler compounds, J. Phys. D: Appl. Phys. **47**, 193001 (2014).
[12] *Heusler Alloys. Properties, Growth, Applications*, edited by C. Felser and A. Hirohata, Springer Series in Materials Science Vol. 222 (Springer International, Switzerland, 2016).
[13] I Galanakis, P. H. Dederichs, and N. Papanikolaou, Slater-Pauling behavior and origin of the half-metallicity of the full-Heusler alloys, Phys. Rev. B **66**, 174429 (2002).
[14] T. Graf, C. Felser, and S. S. P. Parkin, Simple rules for the understanding of Heusler compounds, Prog. Solid State Chem. **39**, 1 (2011).
[15] S.-Y. Lin, M. Chen, X.-B. Yang, Y.-J. Zhao, S.-C. Wu, C. Felser, and B. Yan, Theoretical search for half-Heusler topological insulators, Phys. Rev. B **91**, 094107 (2015).
[16] J. Kübler and C. Felser, Weyl points in the ferromagnetic Heusler compound Co_2MnAl, Europhys. Lett. **114**, 47005 (2016).
[17] Z. Wang, M. G. Vergniory, S. Kushwaha, M. Hirschberger, E. V. Chulkov, A. Ernst, N. P. Ong, R. J. Cava, and B. A. Bernevig, Time-Reversal Breaking Weyl Fermions in Magnetic Heuslers, Phys. Rev. Lett. **117**, 236401 (2016).
[18] G. Chang, S.-Y. Xu, H. Zheng, B. Singh, C.-H. Hsu, G. Bian, N. Alidoust, I. Belopolski, D. S. Sanchez, H. Lin, and M. Z. Hasan, Room-temperature magnetic topological Weyl fermion and nodal semimetal states in half-metallic Heusler Co_2TiX (X=Si, Ge, or Sn), Sci. Rep. **6**, 38839 (2016).
[19] K. H. J. Buschow, P. G. van Engen, and R. Jongebreuer, Magneto-optical properties of metallic ferromagnetic materials, J. Magn. Magn. Mater. **38**, 1 (1983).
[20] J. Barth, G. H. Fecher, B. Balke, T. Graf, C. Felser, A. Shkabko, and A. Weidenkaff, Anomalous transport properties of the half-metallic ferromagnets Co_2TiSi, Co_2TiGe, and Co_2TiSn, Philos. Trans. R. Soc. London A **369**, 3588 (2011).
[21] K. Koepernik and H. Eschrig, Full-potential nonorthogonal local-orbital minimum-basis band-structure scheme, Phys. Rev. B **59**, 1743 (1999).
[22] J. P. Perdew, K. Burke, and M. Ernzerhof, Generalized Gradient Approximation Made Simple, Phys. Rev. Lett. **77**, 3865 (1996).
[23] H. J. Monkhorst and J. D. Pack, Special points for Brillouin-zone integrations, Phys. Rev. B **13**, 5188 (1976).
[24] I. Galanakis, K. Özdoğan, and E. Şaşıoğlu, Half-metallic antiferromagnetism in $Cr_{2+x}Se$ ($0 \leqslant x \leqslant 1$): A first-principles study, Phys. Rev. B **86**, 134427 (2012).
[25] H. Ebert, D. Koedderitzsch, and J. Minar, Calculating condensed matter properties using the KKR-Green's function method recent developments and applications, Rep. Prog. Phys. **74**, 096501 (2011).
[26] S. Chadov *et al.* (unpublished).